Heliyon 11 (2025) e41859

Contents lists available at ScienceDirect

Heliyon

journal homepage: www.cell.com/heliyon

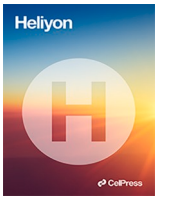

Research article

Determination of radon source in basaltic groundwater, using geochemical tracers and chemometric statistical analysis

Jim Stanley *, Lucy Reading

Queensland University of Technology, 2 George St, Brisbane, Queensland, 4000, Australia

A B S T R A C T

Geochemical tracers such as stable isotopes are widely used in groundwater studies for determining aquifer connectivity and groundwater-surface water interactions. An analysis of dissolved radon (^{222}Rn), major ions and trace element chemistry in groundwater was conducted in the fractured-rock aquifer system of Springbrook plateau, southeast Queensland, Australia. Chemical tracers were used to explore hydrological connectivity between the basalt formation and the underlying rhyolite formation. Water samples were collected from groundwater bores installed in both rock formations, from August 2021 to November 2023. Analysis revealed higher than expected concentrations of radon present in groundwater extracted from the basaltic aquifers (>20 Bq/L). A geochemical analysis of rock samples collected from the plateau, combined with a statistical analysis of water sample chemistry, confirmed the rhyolite formation as the primary source of radon. This indicates a strong hydrological connectivity between the rhyolite and basalt formations, such that the dissolved radon gas in groundwater is easily able to migrate through the network of fractures from the rhyolite formation into the overlying basalt formation. There are indications that seasonal rainfall events may be an important factor controlling the extent of vertical groundwater movement, as shown by temporal changes in radon concentrations. Hence, the groundwater aquifers in both formations should not be considered as discrete, disconnected systems. The geochemical tracers in both water and rock samples used in this investigation, combined with a chemometric statistical analysis, proved to be useful for identifying inter-aquifer connectivity in an area with no previous groundwater investigations.

1. Introduction

The sustainable management of local and catchment-scale groundwater resources requires a detailed knowledge of aquifer and surface water connectivity and groundwater recharge processes [1,2]. This knowledge can be applied to help reduce the over-exploitation of groundwater resources and conserve the condition of groundwater-dependent ecosystems. This is particularly important when considering the potential effects of climate change on the management of environmental resources, and especially in regions where groundwater resources are limited.

The pronounced heterogeneity of fractured-rock aquifer systems can make the detailed characterisation of groundwater flow difficult [3], unless multiple pumping-tests can be conducted across the site, combined with comprehensive outcrop and rock core examination. In heavily vegetated regions with negligible rock outcrop exposures available for the provision of structural information, the application of geochemical tracers provides an especially useful and cost-effective method for examining groundwater connectivity, and groundwater-surface water interaction.

Environmental isotopes, both radioactive and stable, have been employed as tracer techniques in many environmental investigations world-wide [4–10]. Environmental isotopes are a useful tool for studying the exchange of water between groundwater aquifers and surface water [11–14]. When combined with structural and geophysical data, isotope tracer methods provide valuable

* Corresponding author.
E-mail address: j5.stanley@qut.edu.au (J. Stanley).

https://doi.org/10.1016/j.heliyon.2025.e41859
Received 12 June 2024; Received in revised form 5 January 2025; Accepted 9 January 2025
Available online 10 January 2025

information for mapping the extent and connectivity of rock and aquifer formations. However, in some situations, structural and geophysical data may be negligible or absent altogether, placing greater importance on chemical tracer methods.

The naturally occurring isotopes uranium-238 (^{238}U) and thorium-232 (^{232}Th) exist in all rocks and soils in various concentrations [15,16]. Radioactive decay of ^{238}U and ^{232}Th, through a series of shorter-lived radionuclides, produces radium-226 (^{226}Ra) which, in turn, decays by alpha-particle emission to radon-222 (^{222}Rn). ^{222}Rn occurs naturally as a radioactive, colourless noble gas with a half-life of only 3.82 days [17]. The physical ingestion of excess radon can result in serious chronic health problems, such as lung cancer and leukemia [18–22]. Understandably, a significant amount of research has been conducted on monitoring ^{222}Rn concentrations in reservoirs and aquifers which are used for public domestic and drinking water supplies [23–27]. The World Health Organisation and the Australian Drinking Water Guidelines both state a maximum allowable ^{222}Rn concentration of 100 Becquerels per litre (Bq/L) in drinking water [28,29].

In groundwater and surface water systems, higher ^{222}Rn concentrations are associated with igneous rocks which contain naturally higher concentrations of ^{238}U and ^{232}Th, such as granites and rhyolites [15,30,31]. Where groundwater aquifers are formed from, or connected to, these rock types, the radioactive decay of ^{226}Ra results in the continual diffusion of ^{222}Rn into the aquifer pore spaces and fractures, enriching the groundwater with ^{222}Rn, in some cases to concentrations greater than 1000 Bq/L [15,16,29,32,33]. Radium and uranium leached by groundwater from minerals in the source rock are precipitated onto rock fracture surfaces, where they can occur in concentrations greater than within the source rock itself [28,34]. Their radiogenic decay allows for ^{222}Rn to be transported through groundwater flow paths farther away from the source rock. Radon has been applied as a geochemical tracer of submarine groundwater discharge [35–40], as a tool for assessing groundwater-surface water interactions [16], and as a tool for monitoring the effects of seismic events and earthquakes [41–46].

Basalts have much lower natural concentrations of ^{238}U and ^{232}Th than granites [15,21,47], therefore fractured basaltic rock aquifers typically host groundwater with much lower concentrations of dissolved ^{222}Rn [29,48–50]. A review of previous studies shows that radon concentrations measured in groundwater from basaltic fractured rock aquifers tend to be around 4–7 Bq/L, or lower. Table 1 presents a summary from previously published studies of radon concentrations recorded in groundwater from basaltic aquifers. Studies of radon in groundwater do not usually include a comprehensive geochemical or mineralogical analysis to compliment the groundwater analysis so, when outliers are detected, the source of the increased radon concentration at a specific site is open to speculation. It is reasonable to assume that migration of radon and radium from adjacent/nearby formations may be the primary cause for elevated radon concentrations that are sometimes detected in basalt aquifers. Atkins et al. [50] measured a mean radon concentration of 4.90 Bq/L from eighty-eight groundwater samples collected from the fractured basalt formations in the Richmond River Catchment, northern New South Wales. Radon concentrations higher than 10 Bq/L were measured in 5 of the samples, while uranium concentrations in the groundwater were very low (0.04 μg/L).

Cook et al. [51] reported that radon concentrations in groundwater ranged from 6.2 to 125.7 Bq/L. They noted that the higher concentrations were recorded towards the boundaries of the study region where metamorphic rock formations are located, but the possible sources of these higher concentrations were not explored.

Hunt [56] reported a median radon concentration of 104 pCi/L (3.85 Bq/L) from 30 public groundwater supply bores in the basaltic Waianae and Koolau formations (Oahu, Hawaii) and one single outlier of 347 pCi/L (14.69 Bq/L) on the urbanised south coast of the island. The possible cause of the elevated radon concentration, whether natural or anthropogenic, was not examined in an accompanying geochemical analysis.

Luo et al. [54] analysed groundwater samples from 23 monitoring bores in Idaho with a maximum bore depth of 263 m in an underlying basalt formation of approximately 658 m thickness. The average radon concentration in the groundwater samples was 3.03 Bq/L (converted from the dpm/L data), with the two highest measured concentrations being 7.75 and 9.42 Bq/L. The probable geological source of the radon was not investigated.

If a detailed hydro-geochemical assessment is not included when reporting radon concentrations in groundwater from basaltic

Table 1
Summary of selection of previously published radon concentrations in basaltic groundwater aquifers.

Source	Aquifer Type/Geology	Aquifer/Casing Depth	Radon Values (Bq/L)	Location/Country
Segovia et al. [52]	Alluvium & tuff, andesite, basalt and volcanic breccia overlying rhyolite.	35–138 m	(Ave) 2.2	Toluca, Mexico
Cortes et al. [53]	200m thick felsic to intermediate, including rhyolite and basalt.	N/A	<4	Mexico City Basin
Luo et al. [54]	Basalt and interbedded sediments.	Between 60m and 275 m	0.27–9.42	Idaho, USA
Peterson et al. [55]	Vesicular basalt bedrock.	(Upland wells) 105–557.4 m	0.34–5.73	Big Island, Hawaii
Hunt [56]	Fractured basalt.	Shallow (not specified) and deep (23–46 m)	1.48–14.69	Oahu, Hawaii
Lopez et al. [49]	Tertiary igneous rocks including andesite and basalt.	Springs.	0.97–4.99	Mexico
Segovia et al. [48]	Alluvium and basalt.	Not specified.	<7	Mexico
Atkins et al. [50]	Sediments, basalts, sandstone bedrock.	5–120 m	0.14–20.33, (Ave) 4.90	Richmond River Catchment, Australia

aquifers, it is assumed that the dissolved radon is derived from minerals present within the fractured basalt formation, which might not be an accurate assumption. This paper will demonstrate how a geochemical analysis of local lithology, combined with an appropriate statistical analysis of groundwater chemistry data, provides an accurate determination of dissolved radon sources. This greatly assists in groundwater flow path mapping and the management of groundwater resources. The method was applied to investigate aquifer connectivity in a mountainous region characterised by fractured rock hydrology, where only a negligible amount of groundwater data is currently available. The specific rock formations being examined were the Tertiary-age basalt and rhyolite located at Springbrook, Southeast Queensland. Both of these formations are important groundwater reservoirs that make significant contributions to the municipal water supply of the City of Gold Coast and the ecohydrology of protected National Parks.

1.1. Geological and hydrogeological setting

The scenic mountains of the Springbrook National Park are remnants of the northern and western flanks of the Tweed Volcano, which was active approximately 23 million years ago [57,58]. The Tweed Volcano is considered the largest and best-preserved basaltic shield-type volcano in Australia. The numerous lava flows were mostly basalt, but also included explosive eruptions of rhyolite and rhyolitic tuff localised to the Springbrook and Binna Burra areas. The volcano built up to an estimated 2000m in height, the centre of the volcano being present-day Mt Warning in northern New South Wales. From this centre, the lava flows radiated out at an approximate dip angle of 3° [57]. Over time, weathering and erosion have exposed the rock formations and created the current drainage divides and catchment topography.

The uppermost geological unit at Springbrook is the Hobwee Basalt, which ranges in thickness from >100m at its southernmost edge to <40 m at its northern extent. Underlying the Hobwee basalt are two massive rhyolite units: the Springbrook Rhyolite and the Binna Burra rhyolite. The Springbrook rhyolite contacts the overlying Hobwee basalt and has a thickness of up to approximately 100 m which is intercalated by a thin layer of basalt at 70 m depth [57,58]. Beneath the Springbrook rhyolite is the Binna Burra rhyolite unit, which contains rhyolitic tuff [57]. Both rhyolite units have perlitic upper and lower surfaces and are distinctively flow-banded [58]. In the contact region between the Hobwee basalt and Springbrook rhyolite, (ranging from ~805m AHD to ~860m AHD), groundwater is expressed at the surface as several permanent springs which form the headwaters of the creeks which flow along the plateau. During periods of higher rainfall, some ephemeral/seasonal springs also occur, particularly at higher elevations, contributing to surface water flow.

There is a significant lack of historical data available regarding groundwater and groundwater extraction at Springbrook. Presently, there are 19 groundwater bores in the southern section of the Springbrook plateau registered with the Queensland Department of Regional Development, Manufacturing and Water (DRDMW), all occurring on private properties. Historically, there has been no legal requirement for private groundwater bores to be registered, therefore there are potentially more existing groundwater bores, in various states of repair and use, that are not public knowledge. The western side of the Springbrook plateau is steep and heavily forested, being sheltered form the prevailing direction of coastal weathering. This has resulted in nearly all human development taking place on the moderate topography of the exposed rhyolite section on the eastern side of the plateau and therefore no need for groundwater bore installations on the western side. Bore lithology data is available from some bore log records, but no regular sampling and testing of these bores has been conducted to measure standing groundwater levels (SWL) or groundwater quality and chemistry. Historical bore construction data indicates that groundwater is being sourced from the Hobwee basalt and Springbrook rhyolite, with the Hobwee basalt aquifers being the main target for commercial groundwater extraction. No detailed studies have been conducted to explore the physical and chemical properties of the aquifers in these rock units; whether there is mixing between aquifers or whether there are groundwater-surface water interactions.

The region is heavily forested, with very few weathered basalt outcrops observable. Therefore, only general inferences can be made

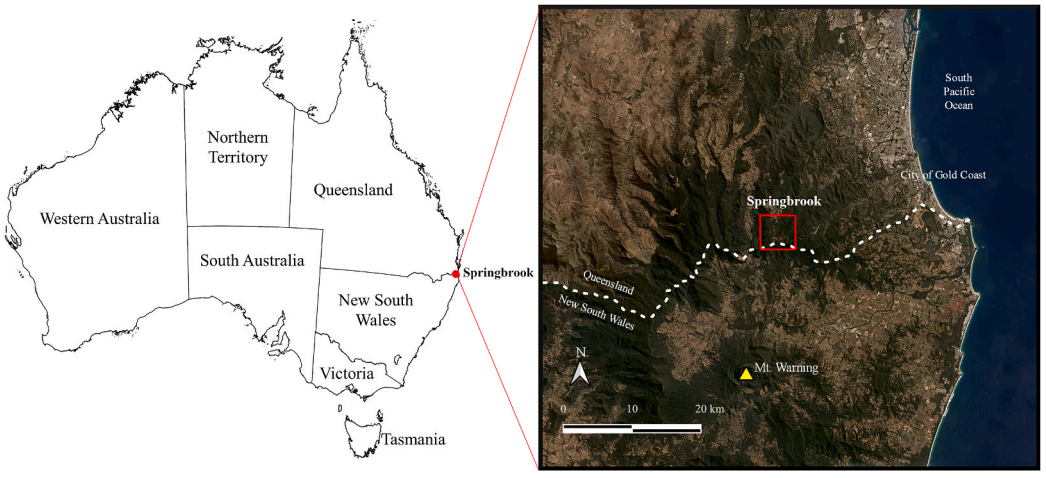

Fig. 1. Location map of Springbrook plateau, in the Gold Coast hinterland, southeast Queensland.

regarding the internal structure of the basalt formation, and no detailed examination can be made without conducting an intensive rock-core drilling program. Given that the weathering of silicate rock minerals influences the chemical characteristics of groundwater, the use of geochemical tracers provides a suitable method for exploring structural components via hydrological components.

2. Materials and methods

2.1. Study area

The Springbrook plateau is located in the Gold Coast Hinterland, Queensland, Australia, approximately 100 km south of Brisbane and 25 km east of Coolangatta [59] (Fig. 1). Springbrook officially covers an area of 30,366 ha, while the upper plateau extends approximately 9.5 kms from north to south, and 3.5 kms from east to west at its widest point. Agricultural land makes up only 1069 ha of the Springbrook area and residential/small farm properties cover 3962 ha [60]. Protected National parks cover approximately 30 % of the area [60]. Elevation above sea level on the plateau itself ranges from 600m to 1010m (AHD), with the Hobwee basalt forming a steep ridge providing a suitable altitude and aspect for a fog and cloud supported permanent rainforest ecosystem. The Springbrook National Park is a declared UNESCO (United Nations Educational, Scientific and Cultural Organization) World Heritage area and is part of the Central Eastern Rainforest Reserves of Australia (CERRA) [61,62]. Historically, Springbrook is one of the wettest places in Queensland, with an average annual rainfall of 2053.5 mm [63]. The only hydrological inputs to the environment are atmospheric: rain, fog, and clouds. For approximately twenty years, commercial groundwater extraction for the production of bottled-water products has been occurring daily at Springbrook.

Bores located at the southern end of Springbrook plateau were selected for monitoring because of the proximity to existing groundwater extraction, waterfalls, creeks and heritage-listed rainforest and national park. Groundwater samples were collected from seven privately owned bores (Fig. 2) every month from August 2021 to November 2023 (with bi-monthly sampling occurring from November 2022 to May 2023). Three of the groundwater bores were assumed to be screened in the Springbrook rhyolite (R1, R2 and R3), and four were assumed to be screened in the Hobwee basalt (B1, B2, B3 and B4). No historical bore logs or lithological data are available for these bores. The depths of the bores and screen locations were verified using a Heron™ Dipper-See submersible camera. Based on their location, and the depth at which their slotted screens inlet groundwater, it is possible that bores B1, B2 and B3 contact the rhyolite formation (Table 2). At a depth of 70 m, it is possible that bore R3 is drawing groundwater from the thin basalt layer that intercalates the Springbrook rhyolite. Bores B1, B3, R1 and R2 intake groundwater from shallow as well as deeper sources, due to being screened at more than one depth location.

Heron™ pressure-transducer data loggers were installed in bores B1, B2, B3, R2 and R3, for the real-time measurement of changes in groundwater levels. The loggers were programmed to record pressure changes every 15 min, and an above-ground barometric logger was used for data compensation. Data loggers were not installed in bores B4 or R1, due to the risk of cable entanglement with the privately owned permanent pumps already installed at those sites. Groundwater was sampled by purging until the water quality parameters stabilised, according to methods defined by Australian Government guidelines [64], using a portable, submersible, 12v

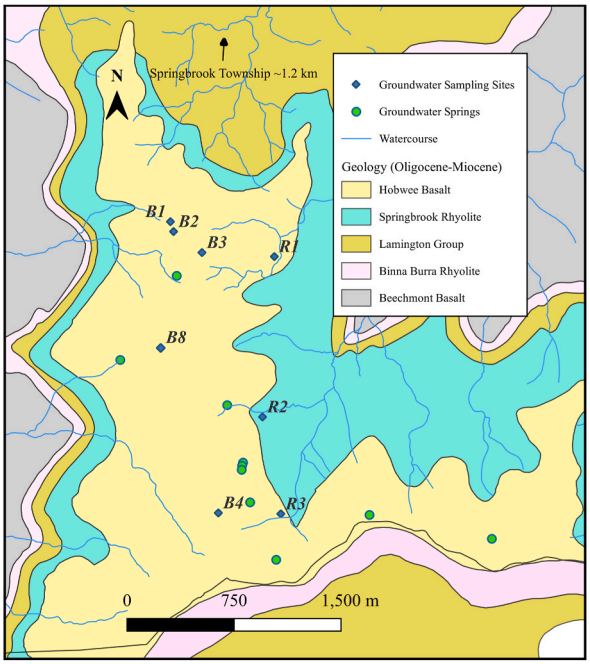

Fig. 2. Geological map of southern Springbrook plateau, showing locations of groundwater bores and springs.

Table 2
List of groundwater bores at Springbrook sampled in this study, including bore depth and screen location. Elevation indicates ground level at bore site, based on Australian Height Datum (AHD).

Site ID	Elevation (mAHD)	Depth (mBGL)	Screens	Formation
B1	785	37	9 m–37 m	Hobwee basalt
B2	803	55	40 m–55 m	Hobwee basalt
B3	815	57	14 m–20 m/46 m–57 m	Hobwee basalt
B4	960	unknown	unknown	Hobwee basalt
R1	767	75	37 m–43 m/55 m–75 m	Springbrook rhyolite
R2	797	26	3 m–7 m/13 m–26 m	Springbrook rhyolite
R3	815	70	50 m–70 m	Springbrook rhyolite

Proactive™ Mega-Monsoon™ pump. At sites B1, R1, R2 and B4, permanent on-site groundwater pumps were present, negating the need for the portable 12v pump at these sites. A portable TPS™ multimeter with submersible probes was used at each site to record pH, electrical conductivity (EC), dissolved oxygen (DO) and oxygen redox potential (ORP).

Water samples intended for radon analysis were collected in 250 mL glass bottles [65]. Samples were collected and analysed for dissolved radon concentrations from August 2021 to November 2023. Samples intended for major ion analysis and trace element analysis were collected at each site in pre-washed polypropylene bottles and vials and filtered using 0.45 μM syringe filters. Samples were transported from Springbrook to Brisbane in a cooler box, refrigerated at $< 3\ ^{\circ}C$. Samples intended for cation analysis and trace element analysis were preserved with double-distilled nitric acid (HNO_3) less than 24 h after sampling. Sample replicates and field blanks of deionised or Milli-Q water were included for quality assurance.

Laboratory analysis of groundwater samples was conducted at the Queensland University of Technology's Central Analytical Research facility (CARF). Radon concentrations in water samples were measured using a portable Durridge Rad7 ™ radon analyser, within 24 h of sampling. Data was later corrected for the effects of radon decay and internal humidity, using the Durridge Capture™ computer software.

Major cations analysis was conducted using Inductively Coupled Plasma Optical Emission Spectroscopy (PerkinElmer Optima ICP-OES). Major anions analysis was conducted using a Dionex Ion Chromatograph (IC). Trace element analysis (including rare-earth elements, lanthanoids and actinoids) was conducted using an Agilent 8900 ICPMS, based on the method by Eggins et al. [66], modified by Lawrence and Kamber [67], Gill et al. [68] and Babechuk et al. [69]. Samples were analysed for trace elements between August 2021 and May 2022. Samples were also analysed for total alkalinity (as $CaCO_3$), using a Mettler-Toledo T50 auto-titrator.

The groundwater major ion chemistry data was then analysed using the ternary diagram method described by Piper [70], to characterise spatial variations in hydrochemistry. Multivariate statistical methods, including hierarchical cluster analysis and numerical correlation coefficient, are widely used to interpret environmental data and are especially useful for understanding changes and relationships between different hydrochemical parameters [71–74]. A chemometric multivariate analysis of groundwater major and trace element chemistry was conducted using Minitab™ statistical software.

A multivariate hierarchical cluster analysis was performed using Complete Linkage method and Correlation Coefficient Distance measurement [75]. The similarities were further quantified by applying a Correlation Coefficient analysis to the same data set. To ensure a reliable analysis, the data was first standardized to "z-scores" for each variable by dividing the difference between each measured value (χ) and mean value (μ) by the standard deviation (δ).

In February 2022, a new groundwater bore (B8) was installed in the Hobwee basalt, using air-hammer drilling method. The bore was completed to a depth of 42 m below ground level (ground level elevation: 903 m AHD), and geological samples were collected from the extracted rock chips corresponding to each 1m interval of depth drilled. For a comparative geochemical study, rock samples of Springbrook rhyolite and Binna Burra rhyolite were collected by hand from outcrops which displayed the least signs of chemical weathering. Rock chip samples extracted from the installation of site B8, and hand-collected samples of Springbrook rhyolite were air-dried, then individually pulverised to powder using a Rocklabs™ Ltd benchtop ring-mill with a tungsten-carbide puck and bowl. Major cations analysis was conducted on pressed discs prepared from powdered samples using Bruker X-Ray Fluorescence (XRF) Spectrometer. Further trace element analysis was conducted on samples using a ESL NWR193 Laser Ablation System, connected to a Agilent 8900 ICPMS. The geochemical certified reference materials (CRM) used in the analysis of rock and soil samples were CRM OREAS 20a (prepared from a I-Type hornblende-bearing granodiorite from the Lysterfield granodiorite complex, south-east Melbourne, Australia), and CRM OREAS 30a (prepared from unweathered olivine tholeiitic basalt from the Quaternary Newer Volcanics Province in Victoria, Australia) (ORE Research & Exploration Pty Ltd).

Rainfall data for Springbrook was sourced from the Australian Bureau Of Meteorology (BOM) [63]. The BOM has two rainfall gauges installed at Springbrook (040607 and 040848), which provide daily rainfall amounts in millimetres. Average monthly rainfall was calculated using combined data from both BOM rain gauges.

3. Results

3.1. Water sample chemistry–radon

Radon concentrations in groundwater ranged from 0.13 Bq/L to 101.09 Bq/L over the study period. The highest concentrations of radon in groundwater were detected in R1 and R2 (Table 3), both of which are bores installed in the Springbrook rhyolite. Only in bore

R1 did radon concentrations exceed the maximum acceptable consumption level of 100 Bq/L [28,29], in September 2023 (Table 3). The spatial variation in average radon concentrations for each groundwater site are presented in Fig. 3. Bore R3, which draws groundwater from 50 m–70 m depth in the rhyolite formation, displayed lower concentrations than R1 and R2. When comparing the radon concentrations to rainfall data, it was observed that radon concentrations in R3 increased in response to rainfall events (Fig. 4A). This same trend was observed in bores B3 and B4, which are installed at a higher elevation on the basalt ridge. In bores B1, B2, R1 and R2, a decrease in radon concentrations was observed in response to rainfall events (Fig. 4B and C).

3.2. Groundwater levels

Data loggers installed in bores B1, B2, B3, R2 and R3 provided groundwater level data for the entire study period, however some data loss ocurred at bore R3 due to data logger malfunction (July–October 2022). Fig. 5 displays groundwater level (GWL) data combined with rainfall data from the BOM. A distinctly rapid groundwater level response to rainfall events can be observed in sites B1 and B2, with groundwater levels rising over 5m during single rain events, and rising overall by more than 15 m. Groundwater responses to rainfall events can be observed in the other bores, but these responses were smaller.

Data loggers installed in bores B1, B2, B3, R2 and R3 provided groundwater level data for the entire study period, however some data loss ocurred at bore R3 due to data logger malfunction (July–October 2022). Fig. 4 displays groundwater level (GWL) data combined with rainfall data from the BOM. A distinctly rapid groundwater level response to rainfall events can be observed in sites B1 and B2, with groundwater levels rising over 5m during single rain events, and rising overall by more than 15 m. Groundwater responses to rainfall events can be observed in the other bores, but these responses were smaller.

3.3. Water sample chemistry–major ions and trace elements

The dominant major ions in groundwater at Springbrook were Ca^{2+}, Mg^{2+}, K^{+}, Na^{+}, $CaCO_3$ and Si^{4+}. Fe^{2+} occurred in very low concentrations (μg/L), except for at site R3, the only groundwater site which consistently showed any Fe^{2+} concentrations above 0.02 mg/L (Table 4). R3 also had the highest average Mn^{2+} concentrations out of all groundwater sites (1.07 mg/L). Piper ternary diagram viasualisation characterised sites B3, B4 and R3 as Ca-Mg-HCO_3 water type (Fig. 6). Sites B1, B2, R1 and R2 were typically characterised as Na-Cl water type, with the samples from these bores occasionally displaying a mixed water type.

Most trace elements in the groundwater samples occurred in concentrations less than 1 μg/L. Trace elements with the highest concentrations included U^{4+}, Sr^{2+}, Rb^{+}, V^{5+}, Pb^{2+}, Th^{4+}, Cs^{+} and Sc^{3+}.

3.4. Statistical analysis of groundwater samples

The results of the hierarchical cluster analysis (HCA) of groundwater chemical variables showed two distinct clusters: Ca^{2+}, Mg^{2+}, Sr^{2+}, V^{5+}, $CaCO_3$, Na^{+}, Si^{4+}, Sc^{3+} and Cr^{2+} in the first (blue) cluster, and K^{+}, Rb^{+}, Cs^{+}, Radon, U^{4+}, Th^{4+} and Pb^{4+} in the second (red) cluster (Fig. 7). Both Cr^{2+} and Pb^{4+} show less similarity to the two clusters (49.54 % and 51.86 %, respectively).

The statistical trends observed in HCA were also observed in the correlation analysis (Table 5). In particular, Ca^{2+} was found to correlate strongly with Mg^{2+}, Sr^{2+}, $CaCO_3$ and V^{5+}, and K^{+} was found to correlate strongly with Rb^{+}, Si^{4+}, Cs^{+} and radon.

3.5. Rock sample chemistry

Geochemical data from rock powder analysis showed that the basalt samples had higher average major ion concentrations of Ca^{2+} (7.41 ppm) and Mg^{2+} (4.60 ppm), compared to the rhyolite samples (0.27 ppm and 0.06 ppm, respectively). The rhyolite samples showed higher average concentrations of K^{+} (5.23 ppm) and Si^{4+} (71.90 ppm), compared to the basalt samples (0.91 ppm and 51.78 ppm). Na^{+} concentrations showed only slight variation between the two rock types (average Na^{+} concentration in basalt samples was 3.42 ppm, and 2.99 ppm in rhyolite samples).

The results of the trace element analysis show that the basalt samples had higher concentrations of V, Cr^{2+}, Sr^{2+} and Sc^{3+}, compared to the rhyolite samples, while the rhyolite samples had higher concentrations of Rb^{+}, Th^{4+}, Cs^{+}, U^{4+} and Pb^{4+} (Fig. 8).

4. Discussion

4.1. Groundwater chemistry

Although no bore log data is available to confirm the lithology of each groundwater bore, the major and trace element data provides distinct geochemical signatures for basalt vs rhyolite. Not surprisingly, the highest radon concentrations occurred in two bores that are installed in the Springbrook rhyolite: R1 and R2. The consistency of the higher radon concentrations in these bores suggests that the groundwater is predominantly drawn from aquifers in the rhyolite, with negligible mixing of water from basaltic aquifers. This is supported by their chemical classification within the Na-Cl and Na-K-HCO_3 fields on the Piper ternary diagram, as the groundwater derived from the basaltic aquifers is of the Ca-Mg-HCO_3 type. R1 and R2 also display lower Ca^{2+} and Sr^{2+}

concentrations (and higher Rb^{+} and U^{4+} in R1) in the hydrochemistry analysis, which indicates a hydrochemistry influenced by a rhyolitic aquifer mineralogy.

Although R3 is also installed in the rhyolite, it showed lower radon concentrations than the neighbouring R1 and R2, and also had

Table 3
Monthly radon concentrations measured from samples collected at each groundwater site, including standard deviation (SD) and calculated average radon values for each site. (N/A indicates that site was unavailable for sampling at that time).

		B1	SD	B2	SD	B3	SD	B4	SD	R1	SD	R2	SD	R3	SD
2021	**August**	8.18	0.94	0.52	0.17	8.74	0.71	1.07	0.41	55.98	1.85	33.45	0.75	0.13	0.08
	September	21.68	1.34	14.87	0.99	2.74	0.43	3.58	0.50	76.10	1.87	43.10	2.32	5.25	0.65
	October	2.39	0.81	6.55	0.73	4.16	0.76	5.11	0.71	79.53	2.61	39.72	2.65	3.73	0.33
	November	12.23	1.20	0.78	0.13	6.90	0.69	3.70	0.75	74.29	2.02	51.49	3.95	11.11	1.12
	December	9.06	0.82	N/A	N/A	14.39	1.44	6.10	0.93	42.80	1.93	4.46	0.37	18.82	0.94
2022	**January**	N/A	N/A	N/A	N/A	9.81	1.36	7.28	0.50	22.59	2.39	N/A	N/A	15.29	1.54
	February	13.62	0.60	0.84	0.34	6.40	0.37	9.27	1.06	75.10	2.44	7.32	0.84	25.80	1.04
	March	10.50	0.71	0.70	0.24	17.04	1.60	12.43	0.55	65.88	1.86	26.63	1.81	21.38	1.69
	April	9.12	1.16	0.84	0.27	6.12	1.12	5.16	1.11	44.47	2.24	56.10	1.59	5.74	0.60
	May	7.60	1.48	4.04	0.48	13.38	0.74	9.62	0.82	32.05	2.25	58.81	2.71	17.86	1.78
	June	14.62	1.08	0.31	0.19	14.75	0.76	12.81	0.51	82.81	2.21	29.75	1.84	8.60	0.57
	July	19.90	0.98	9.82	0.69	13.59	1.18	8.84	0.40	76.49	2.04	13.12	1.09	4.25	1.74
	August	15.34	1.09	N/A	N/A	14.75	N/A	9.33	0.68	81.27	4.28	N/A	N/A	N/A	N/A
	September	16.61	2.36	N/A	N/A	N/A	N/A	6.54	0.90	80.90	2.97	42.21	2.42	2.49	0.49
	October	9.17	0.89	3.51	0.23	12.40	0.76	3.69	0.42	70.67	4.08	N/A	N/A	4.36	0.49
	December	17.39	0.96	0.07	0.10	8.99	0.74	5.95	0.49	76.22	5.48	38.60	2.14	2.76	0.49
2023	**February**	15.95	0.95	8.60	0.44	11.81	1.70	3.80	0.16	66.09	2.87	58.81	1.36	10.34	1.07
	April	9.95	1.12	0.27	0.14	11.67	0.67	7.61	0.88	51.79	2.27	54.42	2.19	10.01	1.13
	June	12.54	1.14	0.61	0.35	13.08	1.23	4.78	0.53	95.17	3.56	43.24	2.70	9.50	0.76
	July	15.05	1.50	0.11	0.10	6.79	0.54	3.97	0.68	65.50	0.85	24.01	1.08	11.51	1.06
	August	23.89	1.40	19.67	1.66	10.65	0.91	6.59	0.80	93.81	1.67	51.18	1.03	6.73	0.52
	September	17.23	1.33	1.30	0.31	5.78	0.49	3.79	0.64	101.09	3.43	50.14	2.33	11.31	0.79
	October	27.94	1.10	18.81	1.27	1.37	0.32	6.42	0.95	97.06	4.34	47.72	2.19	12.89	1.41
	November	31.17	1.70	25.42	2.62	0.57	0.13	6.62	0.99	91.21	3.29	55.45	0.90	5.72	0.78
	Average:	*14.83*		*5.88*		*9.39*		*6.42*		*70.79*		*39.51*		*9.81*	

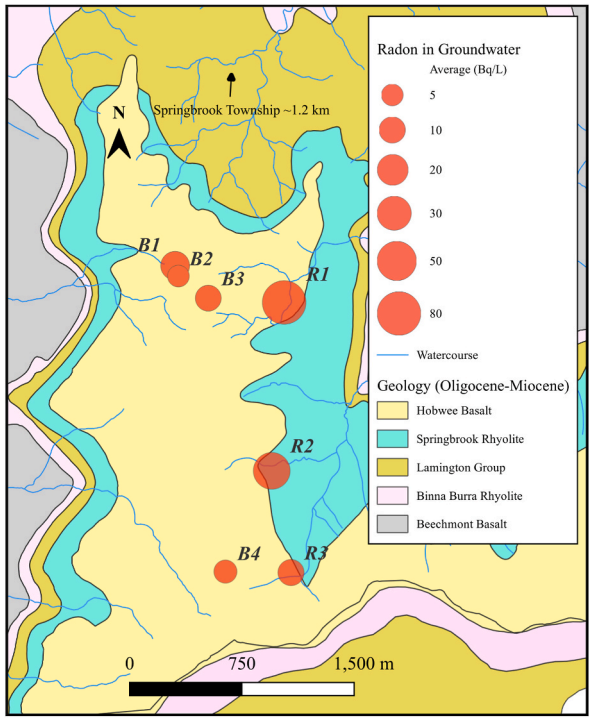

Fig. 3. Displaying spatial variance in average radon concentrations (Bq/L) for each groundwater site.

higher Sr^{2+} and $CaCO_3$ concentrations. On the Piper diagram, R3 is chemically classified within the Ca-Mg-HCO_3 field. In light of these correlations, it possible to conclude that R3 is drawing groundwater from the basalt layer which intercalates the Springbrook Rhyolite at a depth of 70 m.

The temporal dynamics of the radon concentrations in R3 display the same trend as B4, which is located above R3 at a higher elevation on the basalt ridge. The radon concentrations in both bores begin with low concentrations at the start of the study period, then increase to peak in March 2022 before showing a decline. It is worth noting that the study commenced at the start of a La Nina climatic event on the east coast of Australia, with heavy rains beginning in September 2021 (coinciding with radon increase in R3 and B4), increasing in October 2021 and peaking in late February 2022 (BOM). An increase in radon concentrations following rainfall can also be seen in bore B3, with a radon peak of 17.04 Bq/L in March 2022. The higher Sr^{2+}, Cr^{2+} and V^{5+} concentrations, combined with the Ca-Mg-HCO_3 classification on the Piper diagram, indicate B3 has a basaltic groundwater signature, with the increase in radon concentrations signifying a connection to underlying rhyolite aquifers. In bores B3, R3 and B4 it is possible that the increasing radon concentrations are a result of rhyolite aquifers becoming fully saturated from significant rainfall events, increasing the dispersion of dissolved radon gas through saturated fracture zones. Previous studies have observed increases in radon concentrations following rainfall: Smetanova et al. [76] recorded seasonal increases in groundwater levels and groundwater radon concentrations following rainfall events, in fractured quartzite aquifers; De Francesco et al. [77] recorded increases of radon concentrations in groundwater of up to two orders of magnitude during wet season rainfall in southern Italy, and Maeng et al. [78] observed radon concentrations in soil also increased following rainfall. While the geology of these sites was different to that of Springbrook, the principle of increased radon mobility driven by saturation is essentially the same.

There are also indications of radon concentrations increasing in sites R2 and R3 following rainfall events. It would be worthwhile to continue monitoring these bores to determine whether or not the radon concentrations in the bores would decrease to lower concentrations during extended periods of dry weather.

Although bores B1 and B2 are installed on the lower ridge of the Hobwee basalt formation, their depths and screen locations suggest that these bores are drawing water from within the Springbrook Rhyolite. However, there were significant fluctuations in the radon concentrations, which were much lower than those in R1 and R2. The groundwater in B2, in particular, had very low radon concentrations, compared to other the sites. There was an increase in radon concentrations in September 2021, but the levels declined significantly in the following months. Converse to the radon activity observed in B3, R3 and B4, this appears to be radon dilution due to rainfall, in B1 and B2 [79–82]. This dilution of radon may be influenced by a consistent recharge of low-radon groundwater from the overlying basaltic aquifers. The groundwater level data displayed in Fig. 4 shows how responsive these two sites are to rainfall, with groundwater levels rapidly increasing during rain events, followed by a similar groundwater level decline. This indicates a strongly fractured aquifer network within this section of the mountain, allowing for a quick recharge and discharge of groundwater moving through the basalt. In contrast, other sites (R2, R3, B3) show fairly steady groundwater levels throughout the duration of the study period (Fig. 4), indicating a constant steady recharge, and saturation of, aquifers within the rhyolite formation.

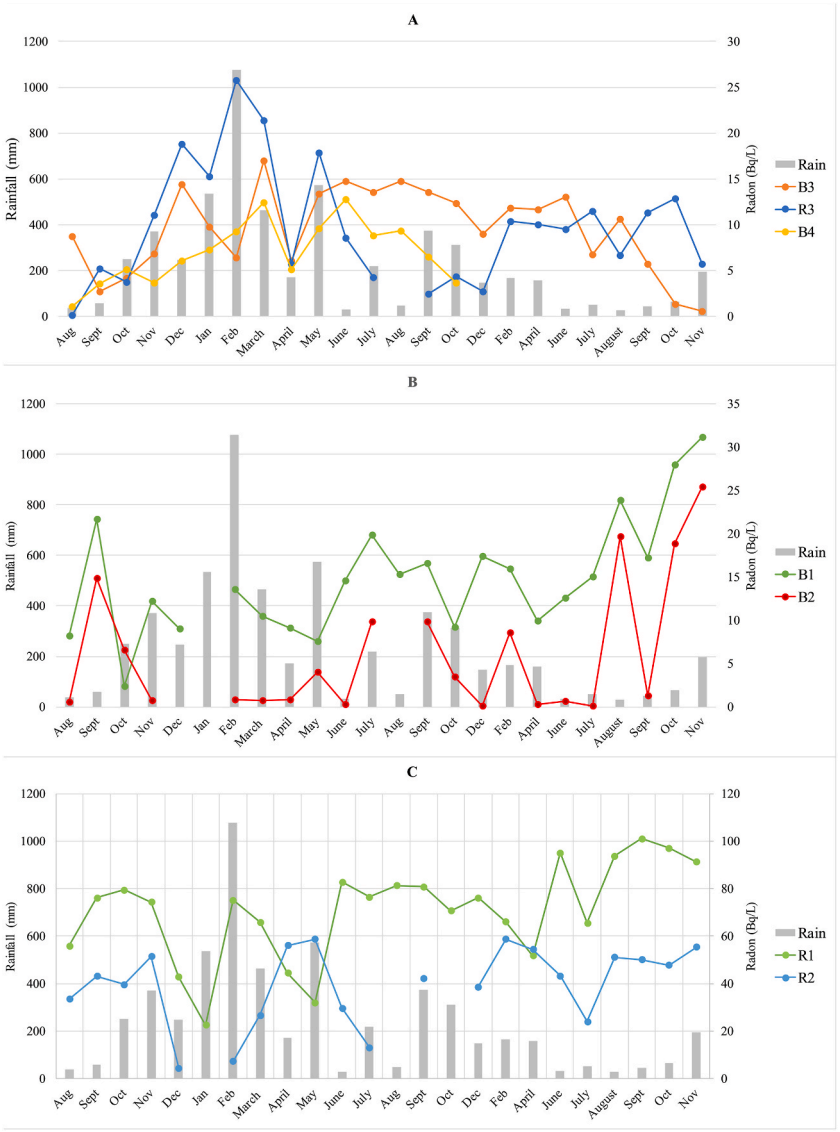

Fig. 4. Monthly radon concentrations in groundwater combined with monthly rainfall data. The data has been presented in three figures for the ease of visualisation and to demonstrate temporal changes in radon concentrations: Fig. 4A displays groundwater sites where radon concentrations in groundwater increased with rainfall events (B3, B4 and R3); Fig. 4B and C displays sites where radon concentrations in groundwater decreased with increased rainfall (B1, B2, R1 and R2).

4.2. Geochemistry and statistical analysis of groundwater

The Springbrook plateau is composed of two geochemically distinct igneous rock types, and their elemental variance was apparent in the results of the major and trace element analysis of rock samples. Compared to the rhyolite samples, the basalt samples had higher concentrations of Ca^{2+}, Cr^{2+}, Mg^{2+}, Sr^{2+}, V^{5+} and Sc^{+}, while the rhyolite had noticeably higher concentrations of K^{+}, U^{4+}, Pb^{4+}, Th^{4+}, Rb^{+} and Cs^{+}. Na^{+} concentrations in the Hobwee basalt and Springbrook rhyolite were similar, which could be due to the presence of Na-enriched feldspars like andesine, oligoclase and labradorite ($(Ca,Na(Al,Si)_4O_8$) [54].

The predominance of Ca^{2+} and Mg^{2+} in the Hobwee basalt can be explained by the presence of Mg-rich olivine, Ca/Mg pyroxenes, such as Ca-rich augite, and Ca-enriched labradorite [83]. Sr^{2+} easily substitutes for Ca^{2+} in feldspars and other Ca-rich minerals [83], which explains its higher concentration in the basalt, compared to the rhyolite. Basalts also typically contain higher concentrations of Sc^{3+} than rhyolites, due to its substitution for Fe^{3+} in pyroxenes [84–86]. Similarly, Rb^{+} readily substitutes for K in potassium feldspars, explaining its higher concentration in the rhyolite (as sanidine; [57]). Cs^{+} also substitutes for K^{+} in micas and feldspars [86,87], hence its higher occurrence in the rhyolite samples. The higher Pb^{4+} in the rhyolite samples may be demonstrative of its occurrence as a radiogenic decay product of U and Th [88].

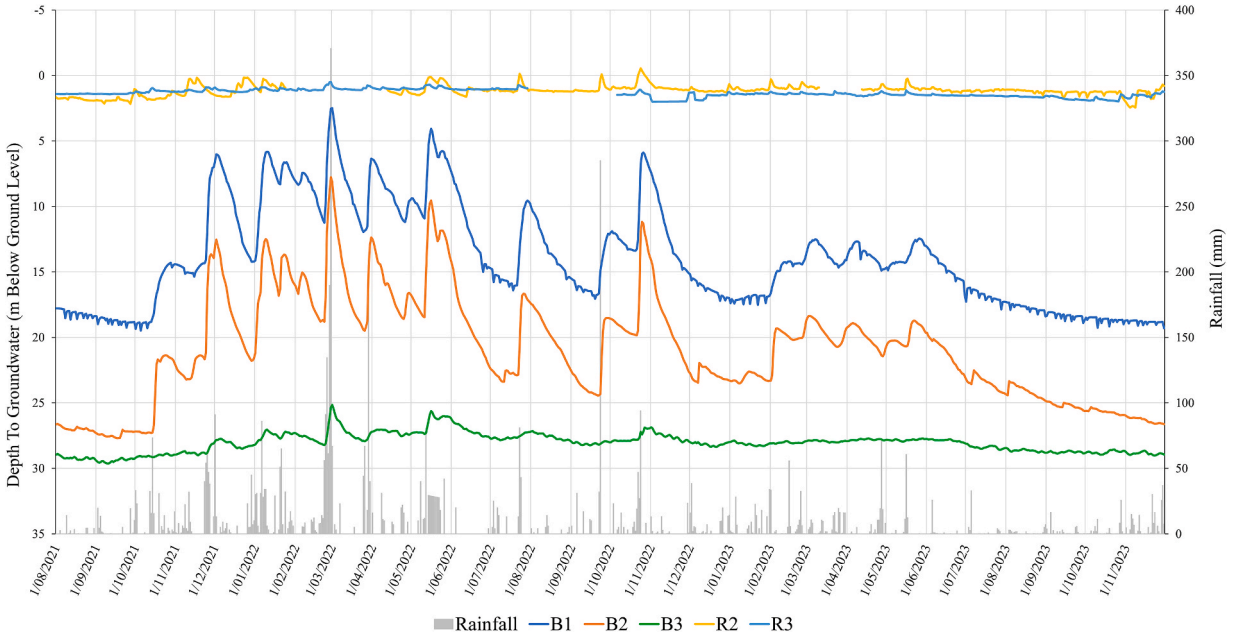

Fig. 5. Springbrook groundwater levels and rainfall data.

Table 4
Calculated average concentrations of major and trace elements in groundwater samples.

	B1	B2	B3	B4	R1	R2	R3
$CaCO_3$ (mg/L)	7.16	14.17	22.04	58.47	11.27	5.45	35.07
Ca (mg/L)	1.26	3.35	3.51	10.92	1.33	1.14	3.42
Mg (mg/L)	1.23	1.73	3.01	5.32	1.15	0.85	1.88
K (mg/L)	0.15	0.81	0.64	1.15	2.54	0.86	0.69
Na (mg/L)	5.01	6.64	6.57	8.49	7.71	4.09	4.37
Si (mg/L)	5.43	7.02	10.89	19.22	16.50	5.63	5.28
Al (mg/L)	0.04	0.02	0.03	0.00	0.05	0.05	0.01
Fe (µg/L)	6.90	0.49	0.56	7.47	3.20	46.00	
Fe (mg/L)							7.86
Cl (mg/L)	5.86	6.84	5.47	6.49	8.08	5.68	5.47
SO_4 (mg/L)	1.20	1.20	1.38	1.20	1.32	2.56	0.81
V (µg/L)	0.08	0.34	1.31	5.79	0.09	0.02	0.17
Cr (µg/L)	0.34	0.21	1.50	0.36	0.19	0.10	0.26
Cs (µg/L)	0.06	0.08	0.04	0.01	0.33	0.11	0.10
Sc (µg/L)	0.27	0.42	0.64	0.89	0.83	0.34	0.40
Rb (µg/L)	0.45	2.41	1.57	2.28	10.46	2.97	2.62
Sr (µg/L)	9.88	13.15	31.90	66.51	6.78	6.18	23.51
Pb (µg/L)	0.54	1.45	0.01	0.44	1.09	2.42	0.003
Th (µg/L)	0.02	0.01	0.02	0.01	3.87	0.02	3.24
U (µg/L)	0.71	33.87	1.46	5.39	115.25	28.66	1.78

The geochemical signature of both rock types was evident in the statistical cluster analysis of groundwater samples to a level of four clusters, with the major geochemical variables diverging into two main groups. The 1st (blue) cluster (Fig. 5) displayed a strong representation of the geochemical elements which had higher concentration in the basalt rock samples (Ca^{2+}, Mg^{2+}, Sr^{2+}, V^{5+}; similarity >93 %), whereas the 2nd (red) cluster contained the elements which had higher concentrations in the rhyolite rock samples (K^{+}, Rb^{+}, U^{4+}, Th^{4+}). The chemical weathering of Ca-rich mafic minerals results in the mineralisation of calcite ($CaCO_3$) in fractures and voids within basalt [83,89,90], hence the strong correlation between the occurrence of Ca^{2+} and $CaCO_3$.

There was strong similarity between K^{+}, Rb^{+} and Cs^{+} (92.33 %), indicating their mineralogical origin from the chemical weathering of feldspar minerals in the rhyolite. The radon occurred in the red cluster, at a similarity level of 81.35 % to K^{+} and Rb^{+}. The correlation matrix showed a negative correlation between radon and the basaltic geochemical elements (Ca^{2+}, Mg^{2+}, Sr^{2+}, $CaCO_3$, V^{5+} and Cr^{2+}). This identifies the rhyolite as the principal source of radon at Springbrook, indicating that the radon detected in groundwater within the basalt formation is the result of vertical dispersal of dissolved radon through rock fractures, into the overlying basalt aquifers. The outcome of this process is that the radon concentrations are sometimes higher than the typical range expected from

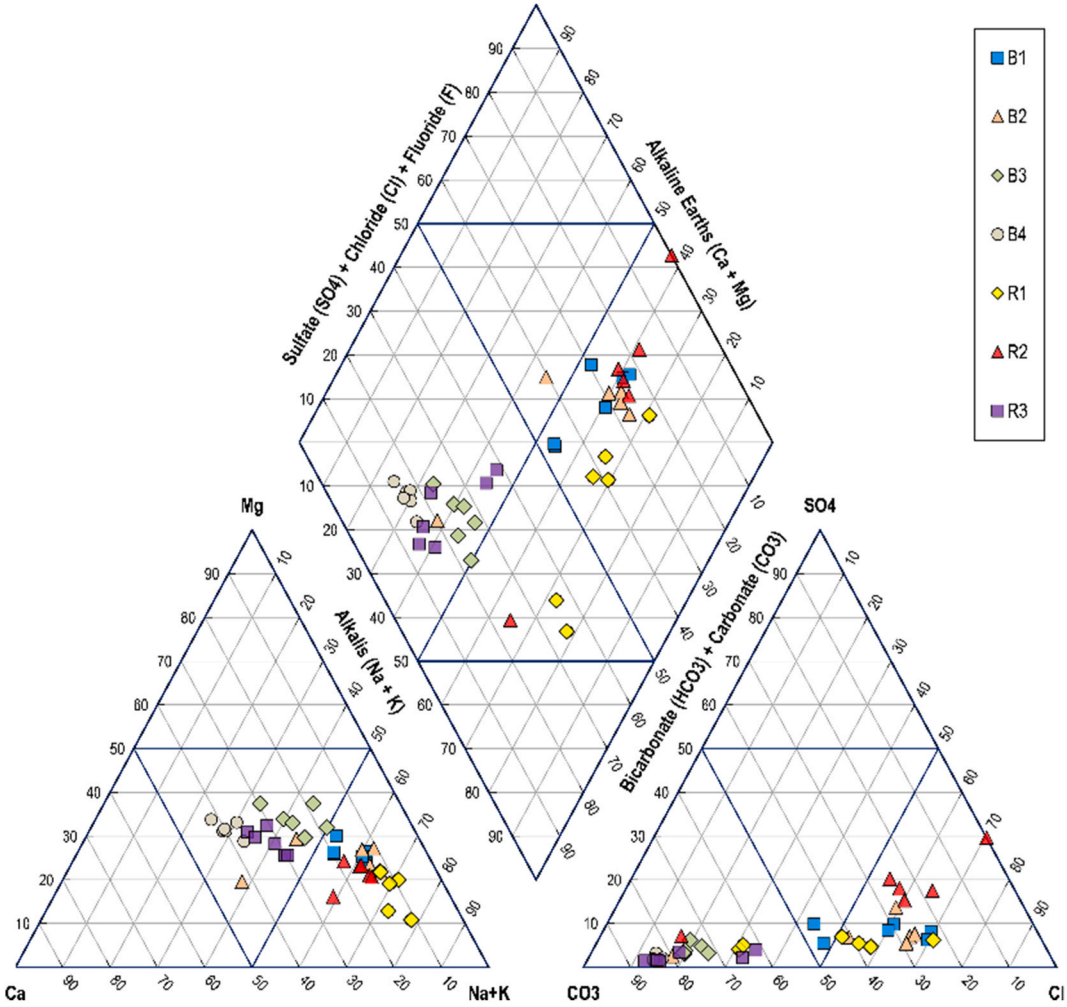

Fig. 6. Piper diagram showing major ion chemical characterisation of groundwater sites.

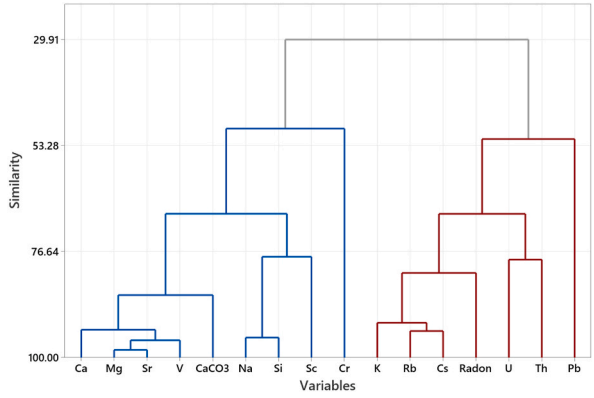

Fig. 7. Results of hierarchical cluster analysis of chemical elements in groundwater samples.

bores installed in a basalt formation.

In other studies that have reported "high" radon concentrations from basaltic aquifers, a more detailed analysis could provide a more precise identification of the radon source. For example, in the Atherton Tablelands region studied by Cook et al. [51], most radon concentrations were higher than 15 Bq/L across the catchment. It is worth noting that the late Tertiary-Quaternary Atherton Basalt

Table 5
Correlation matrix.

	Ca	K	Mg	Na	Radon	Si	$CaCO_{333}$	U	Cr	Sr	Rb	V	Pb	Th	Cs
K	0.291														
Mg	**0.925**	0.131													
Na	0.614	0.572	0.571												
Radon	−0.300	**0.627**	−0.351	0.061											
Si	0.639	**0.760**	0.545	**0.912**	0.261										
$CaCO_3$	**0.842**	0.241	**0.831**	0.479	−0.179	0.537									
U	−0.282	0.508	−0.321	0.149	**0.604**	0.209	−0.289								
Cr	0.069	−0.120	0.296	0.036	−0.209	−0.009	0.136	−0.210							
Sr	**0.898**	0.086	**0.966**	0.463	−0.396	0.484	**0.835**	−0.345	0.273						
Rb	0.005	**0.847**	−0.143	0.433	**0.648**	0.616	0.021	**0.517**	−0.184	−0.166					
V	**0.877**	0.139	**0.923**	0.500	−0.293	0.514	**0.725**	−0.233	0.110	**0.941**	−0.113				
Pb	−0.339	0.037	−0.402	−0.035	0.286	−0.065	−0.351	0.271	−0.331	−0.402	0.096	−0.242			
Th	−0.133	0.473	−0.204	0.166	0.366	0.299	0.020	**0.568**	−0.101	−0.140	0.537	−0.187	0.176		
Cs	−0.152	**0.878**	−0.313	0.325	0.767	0.506	−0.105	**0.659**	−0.235	−0.345	**0.883**	−0.300	0.176	0.598	
Sc	0.453	0.740	0.366	0.555	0.289	0.724	0.422	0.210	0.086	0.382	0.570	0.397	−0.121	0.311	0.507

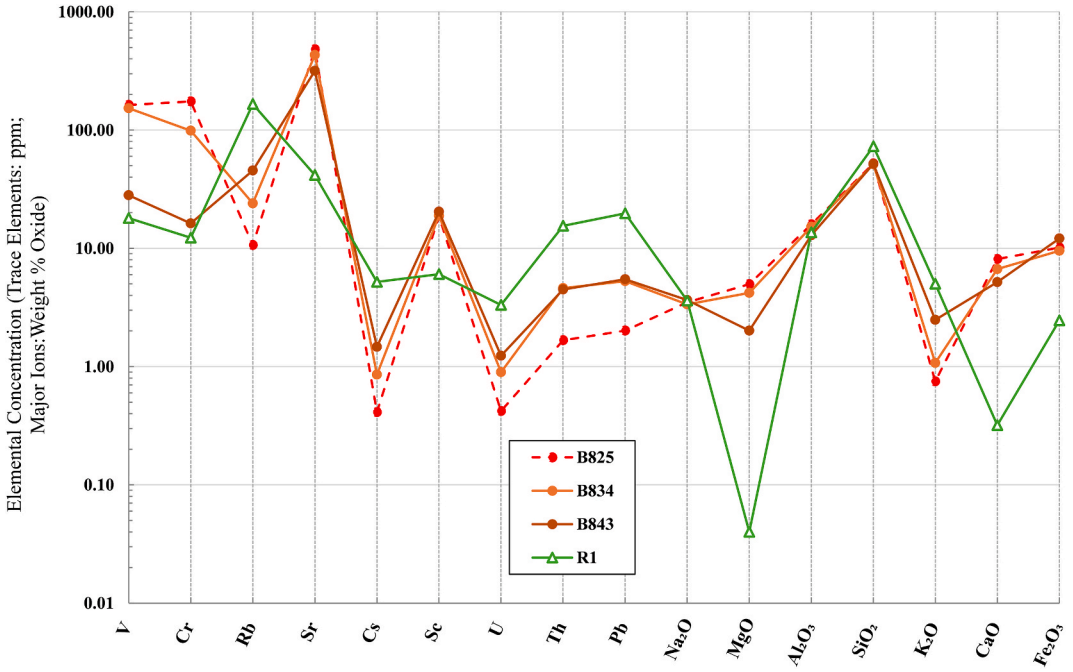

Fig. 8. Major and trace element concentrations in rock samples. B825, B834 and B43 = Hobwee basalt. R1 = Springbrook rhyolite. Major ions are reported in weight % oxide, trace elements are reported in ppm.

formation overlies, and is surrounded by outcrops of, the early Permian Watsonville Granite, rhyolitic Walsh Bluff Volcanics, Tinaroo Granite and late Cambrian-early Permian Tully Granite Complex. It is possible that these formations contribute, through hydrological connectivity, to the elevated radon concentration within the fractured rock aquifers of the Atherton Basalt.

Luo et al. [54] reported a maximum measure radon concentration of 9.42 Bq/L from the basalt formation at INEEL in Idaho, but no particular consideration was given to the 2500m of rhyolitic and tuffaceous volcanic rocks that underly the basalt formation. This could have significance for the provenance of the radon, uranium, and thorium isotope activity that was analysed in the groundwater.

In the Richmond River catchment, Atkins et al. [50] did not explore the possibility that the basalt formations might be hydrologically connected through complex fracture systems to the Georgica Rhyolite formation, which is a member unit of the Kyogle Basalt formation, underlying the Lismore Basalt formation [91].

As demonstrated by Vital et al. (2022) [47], fractured bedrock formations with naturally occurring higher uranium concentrations have a high potential to contribute radon to groundwater. Even aquifers composed of volcaniclastic sediments derived from granitic parent material can have high radon emanation potential, due to the smaller particle size enhancing the probability of ^{222}Rn-emanation from the mineral surface into the pore spaces [47].

Therefore, the approach described in this study, where radon analyses were combined with analysis of hydrochemistry and rock geochemistry, using hierarchical cluster and correlation matrix statistical methods, could be readily applied to other locations to more accurately identify radon sources and investigate inter aquifer connectivity.

5. Conclusion

Geochemical tracers have been established as an effective tool for examining groundwater flow paths and sources, especially where structural and geophysical data is limited. This study has provided an insight into the migration of dissolved radon through fractured rock formations, highlighting the structural connectivity between the rhyolitic and basaltic groundwater aquifers.

An analysis of rock samples revealed the geochemical signature of each rock type, and the same elemental relationships were observed in the chemical analysis of groundwater samples. The chemometric analysis showed a strong statistical correlation between radon and the elements which characterised the rhyolite geochemistry (K^+, U^{4+}, Rb^+, Cs^+) and a negative correlation between radon and the elements which characterised the basalt geochemistry ($CaCO_3$, Ca^{2+}, Sr^{2+}, Cr^{2+}, V^{5+}). From these observations, we can be confident that the radon is derived primarily from the chemical dissolution of silicate minerals in the Springbrook rhyolite, and that the lesser amounts of U^{4+} and Th^{4+} present in the Hobwee basalt do not significantly contribute radon to the groundwater.

The groundwater sites chemically characterised as basaltic aquifers (B3, B4 and R3) all showed an increase in radon concentrations following rainfall, as the underlying rhyolite becomes saturated, promoting radon movement. Conversely, the other groundwater sites characterised by higher Na-K and Cl^- (B1, B2, R1 and R2) displayed a decrease in radon concentrations in response to rainfall, as they were recharged with low-radon groundwater from the overlying basaltic aquifers. Hence, the relationship between rainfall events and radon concentrations is indicative of seasonal groundwater movements. It is concerning that some of the radon concentrations

measured in bore R1 crossed the recommended safe drinking threshold of 100 Bq/L. Given that some of the residential properties at Springbrook use groundwater for domestic purposes, it is recommended that further research be conducted, with the cooperation of local landowners, to determine whether dissolved radon levels are presenting a health risk elsewhere in the neighbourhood.

With no lithological data available for each bore, there exists a knowledge gap in the interpreted internal structure of the geological formations, particularly in relation to the location of contact zones between the rhyolite and basalt. However, combining the observed geochemical and hydrochemical data with the known depths and screen locations of each bore allowed a more confident identification of the dominant groundwater source and aquifer type at each bore site.

CRediT authorship contribution statement

Jim Stanley: Writing – original draft, Visualization, Methodology, Investigation, Formal analysis, Data curation. **Lucy Reading:** Writing – review & editing, Supervision, Project administration, Investigation.

Data availability

Data will be made available on request. For requesting data, please write to the corresponding author.

Ethics declaration

The authors declare that this work described has not been published previously and is not under consideration for publication elsewhere. This article's publication is approved by all authors and by the responsible authorities where the work was carried out. If accepted for publication, this article will not be published elsewhere in the same form, in English or in any other language, including electronically, without the written consent of the copyright-holder. All authors involved have made substantial contributions to the conception and design of the study, as well as the acquisition and analysis of data, and the writing and approval of this article for publication.

Declaration of competing interest

The authors declare the following financial interests/personal relationships which may be considered as potential competing interests:Lucy Reading reports financial support was provided by City of Gold Coast. Lucy Reading reports financial support was provided by Queensland Government. If there are other authors, they declare that they have no known competing financial interests or personal relationships that could have appeared to influence the work reported in this paper.

References

[1] K. Sato, Y. Iwasa, Groundwater Hydraulics, Springer, 2006.
[2] R. Doble, G. Walker, R. Crosbie, J. Guillaume, T. Doody, An overview of groundwater response to a changing climate in the Murray-Darling Basin, Australia: potential implications for the basin system and opportunities for management, Hydrogeol. J. 32 (1) (2023) 59–80, https://doi.org/10.1007/s10040-023-02723-5.
[3] P.G. Cook, A guide to regional groundwater flow in fractured rock aquifers. Henley Beach, S. Aust.: CSIRO, Seaview Press, 2003.
[4] J.J. Gibson, T.W. Edwards, S.J. Birks, N.A. St Amour, W.M. Buhay, P. McEachern, D.L. Peters, Progress in isotope tracer hydrology in Canada, Hydrol. Process. 19 (1) (2005) 303–327, https://doi.org/10.1002/hyp.5766.
[5] E. Kalbus, F. Reinstorf, M. Schirmer, Measuring methods for groundwater – surface water interactions: a review, Hydrol. Earth Syst. Sci. 10 (6) (2006) 873–887, https://doi.org/10.5194/hess-10-873-2006.
[6] C. Kendall, J.J. McDonnell, Isotope Tracers in Catchment Hydrology, Elsevier, Amsterdam, 2006.
[7] T. Praamsma, K. Novakowski, K. Kyser, K. Hall, Using stable isotopes and hydraulic head data to investigate groundwater recharge and discharge in a fractured rock aquifer, J. Hydrol. 366 (1–4) (2009) 35–45, https://doi.org/10.1016/j.jhydrol.2008.12.011.
[8] J. Garcia-Orellana, V. Rodellas, J. Tamborski, M. Diego-Feliu, P. van Beek, Y. Weinstein, J. Scholten, Radium isotopes as submarine groundwater discharge (SGD) tracers: review and recommendations, Earth Sci. Rev. 220 (2021) 103681, https://doi.org/10.1016/j.earscirev.2021.103681. J.
[9] T. Strydom, J.M. Nel, M. Nel, R.M. Petersen, C.L. Ramjukadh, The use of radon (RN222) isotopes to detect groundwater discharge in streams draining Table Mountain Group (TMG) aquifers, WaterSA 47 (2 April) (2021), https://doi.org/10.17159/wsa/2021.v47.i2.10915.
[10] M. Schubert, J. Scholten, M. Kreuzburg, E. Petermann, M.L. de Paiva, D. Köhler, M. Schlüter, Radon (222rn) as Tracer for submarine groundwater discharge investigation—limitations of the approach at shallow wind-exposed coastal settings, Environ. Monit. Assess. 194 (11) (2022), https://doi.org/10.1007/s10661-022-10462-5.
[11] J. Midgley, D.F. Scott, Use of stable isotopes of water (D and O-18) in hydrological studies in the Jonkershoek valley, WaterSA 20 (2) (1994).
[12] J. Thomas, T. Rose, Environmental isotopes in hydrogeology, Environ. Geol. 43 (532) (2003), https://doi.org/10.1007/s00254-002-0677-x.
[13] H. Martindale, U. Morgenstern, R. Singh, B. Stewart, Mapping groundwater-surface water interaction using radon-222 in gravel-bed rivers, J. Hydrol. (New Zealand) 55 (2) (2016) 121–134.
[14] F. Navarro-Martinez, A. Salas Garcia, F. Sánchez-Martos, A. Baeza Espasa, L. Molina Sánchez, A. Rodríguez Perulero, Radionuclides as natural tracers of the interaction between groundwater and surface water in the River Andarax, Spain, J. Environ. Radioact. 180 (2017) 9–18, https://doi.org/10.1016/j.jenvrad.2017.09.015.
[15] M. Wilkening, Radon in the Environment, Elsevier, Amsterdam, 1990.
[16] L.D. Cecil, J.R. Green, in: Environmental Tracers in Subsurface Hydrology, Springer Science + Business Media, LLC, New York, 2000, pp. 175–192.
[17] D.D. Pearson, J.M. Danforth, A.A. Goodarzi, Radon (222rn) gas. Reference Module in Biomedical Sciences, 2023, https://doi.org/10.1016/b978-0-12-824315-2.00552-2.
[18] J.D. Appleton, Radon: sources, health risks, and hazard mapping, AMBIO A J. Hum. Environ. 36 (1) (2007) 85–89, https://doi.org/10.1579/0044-7447(2007)36[85:rshrah]2.0.co;2.
[19] J. Tong, L. Qin, Y. Cao, J. Li, J. Zhang, J. Nie, Y. An, Environmental radon exposure and childhood leukemia, J. Toxicol. Environ. Health, Part A B 15 (5) (2012) 332–347, https://doi.org/10.1080/10937404.2012.689555.

[20] G. Degu Belete, Y. Alemu Anteneh, General overview of radon studies in health hazard perspectives, J. Oncol. 2021 (2021) 1–7, https://doi.org/10.1155/2021/6659795.
[21] Y. Manawi, et al., Overview of radon gas in groundwater around the world: health effects and treatment technologies, J. Environ. Manag. 368 (2024) 122176, https://doi.org/10.1016/j.jenvman.2024.122176.
[22] L. Martins, et al., An assessment of groundwater contamination risk with radon based on clustering and structural models, Water 11 (5) (2019) 1107, https://doi.org/10.3390/w11051107.
[23] N. Todorovic, J. Nikolov, S. Forkapic, I. Bikit, D. Mrdja, M. Krmar, M. Veskovic, Public exposure to radon in drinking water in Serbia, Appl. Radiat. Isot. 70 (3) (2012) 543–549, https://doi.org/10.1016/j.apradiso.2011.11.045.
[24] V. Jobbágy, T. Altzitzoglou, P. Malo, V. Tanner, M. Hult, A brief overview on radon measurements in drinking water, J. Environ. Radioact. 173 (2017) 18–24, https://doi.org/10.1016/j.jenvrad.2016.09.019.
[25] S. Bello, R. Nasiru, N.N. Garba, D.J. Adeyemo, Annual effective dose associated with radon, gross Alpha and gross beta radioactivity in drinking water from gold mining areas of Shanono and Bagwai, Kano State, Nigeria, Microchem. J. 154 (2020) 104551, https://doi.org/10.1016/j.microc.2019.104551.
[26] Y. Ajiboye, M.O. Isinkaye, G.O. Badmus, O.T. Faloye, V. Atoiki, Pilot groundwater radon mapping and the assessment of health risk from heavy metals in drinking water of southwest, Nigeria, Heliyon 8 (2) (2022) e08840, https://doi.org/10.1016/j.heliyon.2022.e08840.
[27] M. Poje Sovilj, I. Miklavčić, G. Šmit, D. Stanić, V. Radolić, Estimation of the Annual Effective Dose from Exposure to Radon in Drinking Water in Croatia, 2023, https://doi.org/10.2139/ssrn.4463882.
[28] National Health and Medical Research Council (NHMR), Australian Drinking Water Guidelines 6, 2011, who, Brisbane City, 2011. QLD.
[29] World Health Organisation (WHO), Guidelines for Drinking-Water Quality: Fourth Edition Incorporating the First and Second Addenda, 2022. Geneva.
[30] G. Knutsson, B. Olofsson, Radon content in groundwater from drilled wells in the Stockholm region of Sweden, Nor. Geol. Unders. Bull. 439 (2002) 79–85.
[31] F. Girault, F. Perrier, T.A. Przylibski, Radon-222 and radium-226 occurrence in water: a Review, in: Geological Society, London, Special Publications, 2018, pp. 131–154, https://doi.org/10.1144/sp451.3.
[32] D.P. Loomis, J.E. Watson, D.J. Crawford-Brown, Predicting the occurrence of radon-222 in groundwater supplies, Environ. Geochem. Health 10 (2) (1988) 41–50, https://doi.org/10.1007/bf01758591.
[33] E. Hoehn, H.R. Von Gunten, Radon in groundwater: a tool to assess infiltration from surface waters to aquifers, Water Resour. Res. 25 (8) (1989) 1795–1803, https://doi.org/10.1029/wr025i008p01795.
[34] G. Aekerblom, J. Lindgren, Mapping of Groundwater Radon Potential (IAEA-TECDOC—Fworld Health980), International Atomic Energy Agency (IAEA), 1997.
[35] W.C. Burnett, H. Dulaiova, Estimating the dynamics of groundwater input into the coastal zone via continuous radon-222 measurements, J. Environ. Radioact. 69 (1–2) (2003) 21–35, https://doi.org/10.1016/s0265-931x(03)00084-5.
[36] W.C. Burnett, H. Dulaiova, Radon as a tracer of submarine groundwater discharge into a boat basin in Donnalucata, Sicily, Continent. Shelf Res. 26 (7) (2006) 862–873, https://doi.org/10.1016/j.csr.2005.12.003.
[37] N. Jacob, D.S. Suresh Babu, K. Shivanna, Radon as an indicator of submarine groundwater discharge in coastal regions, Curr. Sci. 97 (9) (2009).
[38] Y. Zhang, H. Li, K. Xiao, X. Wang, X. Lu, M. Zhang, A.A. Wenjing, L. Wan, C. Zheng, X. Wang, X. Jiang, Improving estimation of submarine groundwater discharge using radium and Radon Tracers: application in Jiaozhou Bay, China, J. Geophys. Res.: Oceans 122 (10) (2017) 8263–8277, https://doi.org/10.1002/2017jc013237.
[39] S. Selvam, P. Muthukumar, S. Sajeev, S. Venkatramanan, S.Y. Chung, K. Brindha, D.S. Suresh Babu, R. Murugan, Quantification of submarine groundwater discharge (Sgd) using radon, radium tracers and nutrient inputs in Punnakayal, south coast of India, Geosci. Front. 12 (1) (2021) 29–38, https://doi.org/10.1016/j.gsf.2020.06.012.
[40] S. Zhao, M. Li, W.C. Burnett, K. Cheng, C. Li, J. Guo, S. Yu, W. Liu, T. Yang, N.T. Dimova, G. Chen, Z. Yu, B. Xu, In-situ radon-in-water detection for high resolution submarine groundwater discharge assessment, Front. Mar. Sci. 9 (2022), https://doi.org/10.3389/fmars.2022.1001554.
[41] G. Igarashi, H. Wakita, Groundwater radon anomalies associated with earthquakes, Tectonophysics 180 (2–4) (1990) 237–254, https://doi.org/10.1016/0040-1951(90)90311-u.
[42] J. Planinic, V. Radolic, B. Vukovic, Radon as an earthquake precursor, Nucl. Instrum. Methods Phys. Res. Sect. A Accel. Spectrom. Detect. Assoc. Equip. 530 (3) (2004) 568–574.
[43] F. Ambrosino, L. Thinová, M. Briestenský, C. Sabbarese, Analysis of Radon Time Series recorded in Slovak and Czech caves for the detection of anomalies due to seismic phenomena, Radiat. Protect. Dosim. 186 (2–3) (2019) 428–432, https://doi.org/10.1093/rpd/ncz245.
[44] N. Morales-Simfors, R.A. Wyss, J. Bundschuh, Recent progress in radon-based monitoring as seismic and volcanic precursor: a critical review, Crit. Rev. Environ. Sci. Technol. 50 (10) (2019) 979–1012, https://doi.org/10.1080/10643389.2019.1642833.
[45] C. Papachristodoulou, K. Stamoulis, K. Ioannides, Temporal variation of soil gas radon associated with seismic activity: a case study in NW Greece, Pure Appl. Geophys. 177 (2) (2020) 821–836, https://doi.org/10.1007/s00024-019-02339-5.
[46] S. D'Incecco, E. Petraki, G. Priniotakis, M. Papoutsidakis, P. Yannakopoulos, D. Nikolopoulos, CO2 and Radon Emissions as precursors of seismic activity, Earth Sys. Environ. 5 (3) (2021) 655–666, https://doi.org/10.1007/s41748-021-00229-2.
[47] M. Vital, et al., Factors affecting the radon (222rn) emanation from aquifer rock materials: implications for radiological and groundwater tracer studies, Appl. Radiat. Isot. 189 (2022) 110433, https://doi.org/10.1016/j.apradiso.2022.110433.
[48] N. Segovia, M. Mena, M. Monnin, P. Peña, S. Salazar, J.L. Seidel, E. Tamez, Fluctuations of groundwater radon and chemical species in basaltic aquifers, Radiat. Meas. 28 (1–6) (1997) 741–744, https://doi.org/10.1016/s1350-4487(97)00176-5.
[49] R.N. Lopez, N. Segovia, M.G. Cisneiga, M.B.E. Lopez, M.A. Armienta, J.L. Seidel, P.G. Lopes Pena, M. Loudes Godinez, E. Tamez, Determination of radon, major and trace elements in water samples from springs and wells of northern Mexico State, Mexico, Geofisc. Int. 41 (4) (2002) 407–414.
[50] M.L. Atkins, I.R. Santos, A. Perkins, D.T. Maher, Dissolved radon and uranium in groundwater in a potential coal seam gas development region (Richmond River catchment, Australia), J. Environ. Radioact. 154 (2016) 83–92, https://doi.org/10.1016/j.jenvrad.2016.01.014.
[51] P.G. Cook, A.L. Herczeg, K.L. McEwan, Groundwater Recharge and Stream Baseflow, Atherton Tablelands, QLD: CSIRO Land and Water, Queensland. Brisbane City, 2001.
[52] N. Segovia, E. Tamez, P. Peña, J. Carrillo, E. Acosta, M.A. Armienta, J.L. Iturbe, Groundwater flow system in the valley of Toluca, Mexico: an assay of natural radionuclide specific activities, Appl. Radiat. Isot. 50 (3) (1999) 589–598, https://doi.org/10.1016/s0969-8043(98)00086-4.
[53] A. Cortés, A. Cardona, J. Pérez-Quezadas, S. Inguaggiato, C. Vázquez-López, J.I. Golzarri, G. Espinosa, Radon (^{222}R) in groundwater studies in two volcanic zones of central Mexico, AIP Conf. Proc. (2013), https://doi.org/10.1063/1.4813458.
[54] S. Luo, T.L. Ku, R. Roback, M. Murrell, T.L. McLing, In-situ radionuclide transport and preferential groundwater flows at INEEL (Idaho): decay-series disequilibrium studies, Geochem. Cosmochim. Acta 64 (5) (2000) 867–881, https://doi.org/10.1016/s0016-7037(99)00373-7.
[55] R.N. Peterson, W.C. Burnett, C.R. Glenn, A.G. Johnson, Quantification of point-source groundwater discharges to the ocean from the shoreline of the Big Island, Hawaii, Limnol. Oceanogr. 54 (3) (2009) 890–904, https://doi.org/10.4319/lo.2009.54.3.0890.
[56] C.D. Hunt, Ground-water Quality and its Relation to Land Use on Oahu, Hawaii, 2000-01, U.S. Dept. of the Interior, Honolulu, HI, 2024.
[57] A. Ewart, V.M. Oversby, A. Mateen, Petrology and isotope geochemistry of tertiary lavas from the northern flank of the Tweed Volcano, Southeastern Queensland, J. Petrol. 18 (1) (1977) 73–113, https://doi.org/10.1093/petrology/18.1.73.
[58] W. Willmott, Rocks and Landscapes of the Gold Coast Hinterland, third ed., Geological Society of Australia, Queensland Division, 2010.
[59] E.L. Gray, C.J. Burwell, A.M. Baker, Benefits of being a generalist carnivore when threatened by climate change: the Comparative Dietary Ecology of two sympatric semelparous marsupials, including a new endangered species (Antechinus Arktos), Aust. J. Zool. 64 (4) (2016) 249, https://doi.org/10.1071/zo16044.
[60] Australian Bureau of Statistics (ABS), Region summary: Guanaba – Springbrook dbr.abs.gov.au/region.html?lyr=sa2&rgn=309041241, 2024.
[61] R.J. Hunter, World heritage and associative natural values of the central eastern rainforest Reserves of Australia. Brisbane City, QLD: NSW National Parks and Wildlife Service, 2003.

[62] S.L. Tanner-McAllister, J.R. Rhodes, M. Hockings, A comparison of climate change impacts on park values on four Queensland World Heritage National Parks in Australia, Australas. J. Environ. Manag. 25 (3) (2018) 267–284, https://doi.org/10.1080/14486563.2018.1431158.
[63] Australian Government Bureau of Meteorology (BOM). Available at: http://www.bom.gov.au/.
[64] B. Sundaram, A. Feitz, P. Caritat, A. Plazinska, R. Brodie, J. Coram, T. Ransley, Groundwater Sampling and Analysis – A Field Guide, Geoscience Australia, 2009. Record 2009/27 95pp.
[65] Durridge Company Inc, RAD H2O Radon in Water Accessory for the RAD7 User Manual, 2020.
[66] S.M. Eggins, J.D. Woodhead, L.P.J. Kinsley, G.E. Mortimer, P. Sylvester, M.T. McCulloch, J.M. Hergt, M.R. Handler, A simple method for the precise determination of ≥ 40 trace elements in geological samples by ICPMS using enriched isotope internal standardisation, Chem. Geol. 134 (4) (1997) 311–326, https://doi.org/10.1016/s0009-2541(96)00100-3.
[67] M.G. Lawrence, B.S. Kamber, Rare earth element concentrations in the natural water reference materials (NRCC) nass-5, Cass-4 and slew-3, Geostand. Geoanal. Res. 31 (2) (2007) 95–103, https://doi.org/10.1111/j.1751-908x.2007.00850.x.
[68] L.W. Gill, M.G. Babechuk, B.S. Kamber, T. McCormack, C. Murphy, Use of trace and rare earth elements to quantify autogenic and allogenic inputs within a lowland karst network, Appl. Geochem. 90 (2018) 101–114, https://doi.org/10.1016/j.apgeochem.2018.01.001.
[69] M.G. Babechuk, E.M. O'Sullivan, C.A. McKenna, C. Rosca, T.F. Nägler, R. Schoenberg, B.S. Kamber, Ultra-trace element characterization of the central Ottawa River basin using a rapid, flexible, and low-volume ICP-MS Method, Aquat. Geochem. 26 (4) (2020) 327–374, https://doi.org/10.1007/s10498-020-09376-w.
[70] A.M. Piper, A graphic procedure in the geochemical interpretation of water-analyses, Eos, Trans. Amer. Geophys. Union 25 (6) (1944) 914–928, https://doi.org/10.1029/tr025i006p00914.
[71] K.P. Singh, A. Malik, V.K. Singh, D. Mohan, S. Sinha, Chemometric analysis of groundwater quality data of alluvial aquifer of Gangetic Plain, North India, Anal. Chim. Acta 550 (1–2) (2005) 82–91, https://doi.org/10.1016/j.aca.2005.06.056.
[72] R.D. Gibbons, D. Bhaumik, S. Aryal, Statistical Methods for Groundwater Monitoring, John Willey & Sons, Hoboken, 2009.
[73] D. Gastmans, I. Hutcheon, A.A. Menegário, H.K. Chang, Geochemical evolution of groundwater in a basaltic aquifer based on chemical and stable isotopic data: case study from the northeastern portion of Serra Geral Aquifer, São Paulo State (Brazil), J. Hydrol. 535 (2016) 598–611, https://doi.org/10.1016/j.jhydrol.2016.02.016.
[74] S.T. Catania, L. Reading, Hydrogeochemical evolution of the shallow and deep basaltic aquifers in Tamborine Mountain, Queensland (Australia), Hydrogeol. J. 31 (4) (2023) 1083–1100, https://doi.org/10.1007/s10040-023-02617-6.
[75] T. Spanos, A. En, P. Simeonova, Chemometric expertise of the quality of groundwater sources for domestic use, J. Environ. Sci. Health, Part A 50 (11) (2015) 1099–1107, https://doi.org/10.1080/10934nhmr529.2015.1047646.
[76] I. Smetanová, K. Holý, M. Müllerová, A. Polášková, The effect of meteorological parameters on radon concentration in borehole air and water, J. Radioanal. Nucl. Chem. 283 (1) (2010) 101–109, https://doi.org/10.1007/s10967-009-0128-1.
[77] S. De Francesco, F.P. Tommasone, E. Cuoco, G. Verrengia, D. Tedesco, Radon hazard in shallow groundwaters: amplification and long term variability induced by rainfall, Sci. Total Environ. 408 (4) (2010) 779–789, https://doi.org/10.1016/j.scitotenv.2009.11.024.
[78] S. Maeng, S.Y. Han, S.H. Lee, Analysis of radon depth profile in soil air after a rainfall by using diffusion model, Nucl. Eng. Technol. 51 (8) (2019) 2013–2017, https://doi.org/10.1016/j.net.2019.06.018.
[79] M. Fukui, 222Rn concentrations and variations in unconfined groundwater, J. Hydrol. 79 (1–2) (1985) 83–94, https://doi.org/10.1016/0022-1694(85)90183-0.
[80] F.P. Tommasone, S. De Francesco, E. Cuoco, G. Verrengia, D. Santoro, D. Tedesco, Radon hazard in shallow Groundwaters II: dry season fracture drainage and alluvial fan upwelling, Sci. Total Environ. 409 (18) (2011) 3352–3363, https://doi.org/10.1016/j.scitotenv.2011.05.039.
[81] A. Girija Rengan, S. Joseph, S. Sellamuthu, Seasonal and geological controls of Radon (222 Rn) in groundwater of Vamanapuram River basin, SW India, Geocarto Int. 37 (27) (2022) 18448–18473, https://doi.org/10.1080/10106049.2022.2142961.
[82] J.S. Ibánhez, X.A. Álvarez-Salgado, C. Rocha, Radon prevalence in domestic water in the Ría de Vigo Coastal Basin (NW Iberian Peninsula), Environ. Sci. Pollut. Control Ser. 30 (27) (2023) 69927–69940, https://doi.org/10.1007/s11356-023-27305-6.
[83] K.A. Baublys, S.K. Hamilton, H. Hofmann, S.D. Golding, A strontium (87Sr/86Sr) isotopic study on the chemical evolution and migration of groundwaters in a low-rank coal seam gas reservoir (Surat Basin, Australia), Appl. Geochem. 101 (2019) 1–18, https://doi.org/10.1016/j.apgeochem.2018.12.020.
[84] V.C. Fryklund, M. Fleischer, The abundance of scandium in volcanic rocks, a preliminary estimate, Geochem. Cosmochim. Acta 27 (6) (1963) 643–664.
[85] J.C. Norman, L.A. Haskin, The geochemistry of Sc: a comparison to the rare earths and Fe, Geochem. Cosmochim. Acta 32 (1) (1968) 93–108, https://doi.org/10.1016/0016-7037(68)90089-6.
[86] R. Salminen, Geochemical Atlas of Europe, Geological Survey of Finland, essay, 2005.
[87] J.V. Smith, Feldspar Minerals, Springer-Verlag, 1974.
[88] W.M. White, Geochemistry, first ed., Wiley-Blackwell, 2013.
[89] E.H. Oelkers, S.R. Gislason, J. Matter, Mineral carbonation of CO2, Elements 4 (5) (2008) 333–337, https://doi.org/10.2113/gselements.4.5.333. J.
[90] M.H. Rasool, M. Ahmad, Reactivity of basaltic minerals for CO2 sequestration via in situ mineralization: a Review, Minerals 13 (9) (2023) 1154, https://doi.org/10.3390/min13091154.
[91] M.B. Duggan, D.R. Mason, Stratigraphy of the lamington volcanics in far northeastern New South Wales, J. Geol. Soc. Aust. 25 (1–2) (1978) 65–73, https://doi.org/10.1080/00167617808729014.